arXiv:astro-ph/0004219v1 16 Apr 2000

Structure and Star Formation in NGC 925[1]

D.J. Pisano
Dept. of Astronomy, University of Wisconsin
475 N. Charter St., Madison, WI 53706
`pisano@astro.wisc.edu`

Eric M. Wilcots
Dept. of Astronomy, University of Wisconsin
475 N. Charter St., Madison, WI 53706
`ewilcots@astro.wisc.edu`

Bruce G. Elmegreen
IBM Research Division, T.J. Watson Research Center
P.O. Box 218, Yorktown Heights, NY 10598
`bge@watson.ibm.com`

ABSTRACT

We present the results from an optical study of the stellar & star formation properties of NGC 925 using the WIYN 3.5m telescope. Images in B,V,R, & Hα reveal a galaxy that is fraught with asymmetries. From isophote fits we discover that the bar center is not coincident with the center of the outer isophotes nor with the dynamical center (from Pisano *et al.* 1998). Cuts across the spiral arms reveal that the northern arms are distinctly different from the southern arm. The southern arm not only appears more coherent, but the peaks in stellar and Hα emission are found to be coincident with those of the H I distribution, while no such consistency is present in the northern disk. We also examine the gas surface density criterion for massive star formation in NGC 925, and find that its behavior is more consistent with that for irregular galaxies, than with late-type spirals. In particular, star formation persists beyond the radius at which the gas surface density falls below the predicted critical value for star formation for late-type spirals. Such properties are characteristic of Magellanic spirals, but are present at a less dramatic level in NGC 925, a late-type spiral.

Subject headings: galaxies: individual (NGC 925) – galaxies: spiral – galaxies: structure – galaxies: ISM

1. Introduction

This paper is part of an ongoing series of papers studying the general H I and optical properties of late-type barred spiral galaxies (Sbc-Sd, hereafter LTBS). We will examine the stellar and star forming properties of NGC 925 based on observations from the WIYN 3.5m telescope[2]. We previously observed NGC 925 and NGC 1744, both LTBS, in H I as part of a study of the gaseous properties of this class of galaxies (Pisano *et al.*, 1998, hereafter Paper I), and to determine the pattern speed of their bars (Elmegreen *et al.* 1998). NGC 925 was chosen for study because it is a nearby (∼9.3 Mpc, Silbermann *et al.* 1996), apparently prototypical LTBS which is well oriented in inclination for dynamical and morphological study. This value for the distance will be used throughout this paper.

---

[1] to appear in the August 2000 Astronomical Journal

[2] The WIYN observatory is a joint facility of the University of Wisconsin-Madison, Indiana University, Yale University, and the National Optical Astronomy Observatories.

In paper I, we found that NGC 925 had a weak spiral pattern and bar as indicated by the small streaming motions in the spiral arms and bar. Asymmetries are quite prevalent in NGC 925. NGC 925's southern spiral arm has reasonably coherent streaming motions, while the northern arms do not. The center of the bar is also slightly offset from the dynamical center of the galaxy by ∼950 pc. These asymmetries could possibly be related to the presence of a small H I cloud ($M_{H\ I} \sim 10^7 M_\odot$) interacting with the main galaxy. The strength of the interaction, however, is most likely not enough to drive the asymmetries in NGC 925. The presence of an off-center bar, and a single coherent spiral arm are typically viewed as characteristic properties of barred Magellanic (SBm) galaxies (de Vaucouleurs & Freeman 1972), and have been shown to be potentially long-lasting (Levine & Sparke 1998, Noordermeer *et al.* 2000) While NGC 925 does not illustrate these properties as dramatically as the LMC, for example, it certainly indicates that these characteristic asymmetries do not suddenly appear in SBm's, but are rather a continuous change in morphology throughout late-type disk galaxies. A summary of basic properties of NGC 925 is given in table 1.

LTBS are an understudied and, hence, a poorly understood class of galaxies. While bars may play an important role in galaxy evolution by generating gas inflow (e.g., Matsuda & Nelson 1977, Athanassoula 1992), driving spiral structure (e.g., Sanders & Huntley 1976; James & Sellwood 1978), and flattening the radial abundance gradient (Martin & Roy 1994), these effects are shown to exist primarily in early-type barred spirals (S0-Sb). LTBS do not appear to have strong enough bars to cause such effects (see paper I). Previous studies of LTBS have found that late-type bars tend to have exponential light profiles, as opposed to flat profiles, and end well within corotation, as opposed to just inside it (Elmegreen & Elmegreen 1985, Elmegreen *et al.* 1998). Furthermore, late-type bars are not likely to be driving the spiral pattern (Sellwood & Sparke 1988), in contrast to early-type bars (Elmegreen & Elmegreen 1989). Star formation properties are also different, with late-type bars tending to be gas-rich and have star formation throughout the bar, while early-type bars have star formation only near the ends of the bar (Phillips 1995). Our observations in paper I of NGC 925 provided no evidence to contradict any of these properties.

In this paper, we will investigate the optical properties of NGC 925, with a specific eye towards the nature of star formation in the galaxy. We will see if there are other signatures of asymmetry in NGC 925 that are typically associated with SBm's. Finally, we will try to devine what role the bar plays in determining the properties of the galaxy as a whole. In section 2 of this paper we discuss the observations and reduction. In section 3, we discuss the optical properties of galaxy as a whole. Section 4 discusses the star formation properties of NGC 925 both across the entire galaxy, and in the bar and spiral arms specifically. We conclude in section 5.

2. Observations and Reductions

We observed NGC 925 with the WIYN 3.5m telescope during the nights of October 6 & 7, 1996. The conditions were superb; all three nights had subarcsecond seeing and were photometric. We took the images through the Harris B, V, and R broadband filters and on and off band Hα filters using the WIYN imager, a thinned 2048^2 STIS CCD with 21μm pixels. The pixels correspond to $0.196''$ on the sky. The gain was 2.8 e^- per ADU, and the read noise was 8 e^-. The imager has a total field of view of $6.5'$. Since NGC 925 has a major axis of approximately $10'$, we had to mosaic two images to get full coverage of the galaxy. We observed the east and west sides of the galaxy separately with overlap in the bar region. The parameters of the observations are listed in table 2.

We reduced the data in the usual manner. We took bias images during the afternoon before each night. We visually inspected the biases, and statistically compared them and found them to be identical for all three nights. This being the case, we combined all 44 bias frames into one image for bias subtraction to maximize the signal to noise. Each afternoon, we took ∼5 well exposed (10000-35000 counts) dome-flats per filter. We discarded any flats which were significantly deviant from the average. We averaged the remaining flats together to correct for the response of the CCD. We switched filter wheels during each night's observations which sometimes caused the dust features to change in location and/or intensity. As some of the flats changed between nights, we only used the flats from the same night to flatten the program images. Aside from the off-line Hα images, all images were flat to better than 5%. The off-line Hα images were flat to 10%. The poor quality of the flat-fielding for the Hα-off filter may require sky-flats to improve.

To flux calibrate our images we observed broadband standards in the PG0231+051 and SA92 fields from Landolt (1992), and G191B2B, a spectrophotometric standard from Massey *et al.* (1988). The photometric solutions for the broadband observations were found using the *apphot* package in IRAF. They are as follows:

$$V = OB_V + 1.08 + 0.17 \times X - 0.04 \times (B-V) \quad (1)$$

$$B = (OB_{(B-V)} + OB_V) + 1.28 + 0.22 \times X - 0.04 \times (B-V) \quad (2)$$

$$R = (OB_V - OB_{(V-R)}) + 0.95 + 0.10 \times X - 0.04 \times (V-R) \quad (3)$$

where OB is the instrumental magnitude and X is the airmass. We then applied these solutions to the bias subtracted, flat-fielded, sky subtracted images using IRAF to produce surface brightness maps. The errors on these equations are roughly 0.05 mag. As this is comparable to our flat-fielding errors, we combine the errors to obtain our total error on the broadband magnitudes, which is approximately 0.07 mag.

Sky subtraction was difficult given the small amount of sky present in our images. There was typically only a small corner of the CCD frame which appeared to contain mostly sky emission. For each side of the galaxy we used *imstat* to determine a mean sky level, and subtracted it from the image before mosaicing. This value is quite uncertain given the lack of sky present in the images. Because we were not able to reliably determine the sky values in our images, we did not attempt to determine total magnitudes for NGC 925.

The photometric solutions for the line and continuum images were calculated accounting for the airmass of the observations and the response of the line and continuum filters as determined for our observations of the spectrophotometric standard. Using the respective exposure times and the fractional contribution of the two [NII] lines to the Hα image, we then can get the continuum subtracted Hα image. Based on the spectra in Martin & Roy (1994), we assumed the Hα line accounted for 81% of the emission in the line filter, with the two [NII] lines accounting for 14% and 5% of the emission. We applied these solutions to each filter and each side of the galaxy separately. The line and continuum images were aligned to better than 1 pixel with similar, but not exactly the same, seeing conditions.

Once each image was fully calibrated, we aligned and averaged together the east and west images of NGC 925 to form a total image of the galaxy. To align the images, we identified stars present in both images, calculated the average shift needed to bring the two sides into alignment, and shifted the images using *imshift.* Images were aligned to better than 1 pixel in each dimension. A similar procedure was followed to align the full galaxy B, V, R, and Hα images to each other. At this point we began our analysis. Figure 1 shows our combined B, V, R image of NGC 925.

3. Global Photometric Properties

One of the key thrusts of investigations of late-type spirals is the degree to which their disks are lopsided. Extreme late-types such as the Magellanic spirals have dynamical centers that are significantly offset from the center of the outer isophotes (de Vaucouleurs & Freeman 1972, Odewahn 1996). We can measure a photometric center from our mosaiced image of NGC 925 and a dynamical center from the HI velocity field (Paper 1). NGC 925 is also a barred galaxy, so we can compare the photometric and dynamical center with the apparent center of the bar. Magellanic spirals in particular host bars that are greatly offset from the photometric *and* dynamical centers.

We chose to use the isophote fitting routine in the IRAF package, *ellipse.* We first removed the stars and saturated columns from the image by replacing the central regions of bright stars within a radius of $2.4''$ with the mean from an annulus with inner radius of $3''$ and width $1''$. While some stars were still visible in the image the residuals were only slightly higher than the background level of the galaxy. We fit a series of elliptical annuli $0.''4$ in width to the galaxy. The semi-major axis of each annulus was $4''$ larger than the previous one. The task ceased to produce fits which converged at a radius of $5'$, near the edge of our field of view. We present the results of our elliptical fits in Figures 2 & 3. Note that the scale on the surface brightness plot comes from our photometric calibrations of the background sky level (although this may not be the true sky).

A number of features stand out in the isophotal fits in Figure 2. Overall, the results of the fits are very similar in all bands even though the center, position angle, and ellipticity of the galaxy all vary widely as a function of radius. Within a radius of about $60''$ (i.e. the bar region) the center is fit consistently in all bands. Simply taking the means from each band we define the bar center to be: $2^h24^m17.0^s\pm0.2^s$, $33^o21'15''\pm1''$. The epoch for all of the coordinates in this paper is 1950, unless otherwise stated. There is a sharp change in the fitted declination of the center just beyond a radius of $60''$, coincident with the position of the prominent spiral arm on the southern side of the galaxy. The width of the "bump" in the fitted declination of the center is consistent with the width of the arm. The fitted declination then returns to a value comparable with that derived from the innermost parts of the galaxy. So if we were to ignore the effect of the spiral arm we find that the fitted photometric center of NGC 925 is only slowly varying with radius out to $\sim 170''$ which is close to edge of the optical disk. Beyond about $200''$ the center, position angle, and ellipticity remain relatively constant. While the three bands return inconsistent fits for the center of the galaxy, we take the mean center derived from fits to the annulus $210''$-$270''$ to be the center of the outer isophotes. This yields an isophotal center at $2^h24^m14.8^s\pm0.6^s$, $33^o21'23''\pm2.5''$ which is different from the bar center. Studies of lopsided galaxies usually use the center of the outermost isophotes to define a photometric center of the galaxy (e.g. Odewahn 1991). NGC 925 shows that this center will be a function of the band with which one chooses to carry out the photometry.

The fitted position angle of NGC 925 in Figure 2c slowly increases from -80^o to -55^o from the center to a radius of $180''$; beyond that it drops abruptly. Similar trends are seen in Figure 2d where we plot the fitted ellipticity as a function of radius. It is slowly decreasing from the center out to $180''$ where it also drops abruptly before leveling off. We list our adopted values for the center, position angle, and ellipticity in Table 3

In figure 3a we plot the azimuthally averaged surface brightness distribution for NGC 925. We fit a double exponential to this distribution and we show the residuals in Figures 3b and 3c, respectively. Residuals from our fit solely to the exponential outer-disk (Fig 3b) clearly illustrate the presence of a second exponential at radii within $60''$, and a systematic surface brightness enhancement between $140''$ and $180''$. The latter is much clearer after we subtract our exponential fit to the bar and re-scale the residuals in the lower panel. We chose to fit an exponential to the bar, both because it represents the data well, and because Elmegreen & Elmegreen (1985) found that late-type galaxies including NGC 925 have exponential bars. Both of our fits are shown in the top panel. The derived scale-lengths and central brightnesses for the bar and disk are listed in table 3. One very interesting property illustrated by these scale-lengths is that the disk tends to get redder with increasing radius, as the B scale-length is much smaller than the R scale-length. This is contrary to what is found for most field galaxies (Vennik *et al.* 1996), and could be indicative of a differing star formation history for NGC 925 as compared to most other galaxies. This could also indicate the presence of a very young inner disk and bar in NGC 925.

By looking at all the results of our isophotal fitting, we can pick out some distinct features in NGC 925 which are evident in both a contour plot of the model (figure 4), and in the graphs of the fit parameters (figures 2 & 3). The inner bar region, within $30''$, is characterized by widely varying values for the center, position angle, and ellipticity that are most likely due to patchy star formation and dust in the center of the bar. We get consistent results for the rest of the bar. The southern arm strongly affects the fits in the remainder of the disk. This is evident from the drastic change in center, position angle, and ellipticity at $180''$ where the spiral arm fades (as shown in the surface brightness fits). The slow increase in position angle with increasing radius illustrates the change from the bar dominated region of the galaxy to the region where the spiral arm dominates. Other variations in the fits and surface brightness residuals can be explained by the small scale variations in brightness caused by H II regions and patchy dust within NGC 925.

The bar of NGC 925, based on our fits shown in figure 3, extends out to approximately 60″ (2.7 kpc). It is at this point where the exponential profile of the bar begins to meet the exponential disk. The bar is centered at $2^h24^m17^s$ in right ascension, and $33^o21'15''$ in declination, which is not coincident with the center of the outer isophotes. This is the mean from the isophotal fits of the center within the inner 60″. The bar has an ellipticity of ∼0.69 (b/a = 0.3), and, with a position angle of -75^o, it is aligned within a few degrees of the major axis of the galaxy. The alignment of the bar position angle with the galaxy position angle, and the origination of the spiral arms from the end of the bar may indicate that the bar has had some effect on the disk of the galaxy.

We now have four centers derived for NGC 925: the peak of the brightness distribution (from the RC3), the dynamical center (from Paper I), the center of the bar, and the center of the "outer" isophotes (from above). In figure 5, we compare the locations of these centers as a measure of the asymmetry in the galaxy. The size of the boxes are representative of the fitting errors; the ellipse is the beam size from the H I data used to model the rotation curve. We find that the center of the brightness distribution is nearly coincident with the center of the bar, while the dynamical and outer isophote centers are coincident with each other. The bar center is NOT coincident, however, with either the dynamical or outer isophotal center. This is indicative of an asymmetric galaxy and is quite similar to what is seen in SBm's such as NGC 4618 (Odewahn 1991) which has a 662 pc displacement between the bar center and the center of the outer isophotes. For NGC 925 the dynamical and outer isophotal centers are offset parallel to the bar, whereas most SBm's show bars offset perpendicular to their major axis (Odewahn 1991). NGC 925 may be exhibiting a different type of phenomenon, but this property of SBm's requires further study.

While we were unable to calculate total magnitudes for NGC 925, we used published values for M_B to examine mass-to-light ratios for NGC 925. From the RC3, we find that NGC 925 has an M_B=-19.9 mag. Using the total and H I masses we derived in Paper I, we calculated M_{tot}/L_B to be 5.0, and $M_{H\ I}/L_B$ to be 0.36, consistent with what we expect from its classification as an Scd spiral (Roberts & Haynes 1994), but also similar to values found for later-type spiral galaxies.

4. Star Formation in NGC 925

4.1. Global Properties

In a seminal paper, Kennicutt (1989) observationally examined the dependence of star formation on the properties of the gas in the galaxy. For his study he used the expression for the critical density for a instability to grow in a thin isothermal gas disk:

$$\Sigma_{crit} = \alpha \frac{\kappa c}{3.36G} \qquad (4)$$

where c is the velocity dispersion of the gas, G is the gravitational constant, α is a dimensionless constant near unity which accounts for the deviation of the disk from a thin, isothermal gas disk, and κ is the epicyclic frequency given by:

$$\kappa = 1.41\frac{V}{R}(1+\frac{V}{R}\frac{dV}{dR})^{\frac{1}{2}} \qquad (5)$$

where V is the rotation velocity at a radius R. In our case the rotation curve is given by a Brandt rotation curve derived from a fit to the H I data in paper I:

$$V(R) = \frac{V_{max}}{R_{max}}\frac{R}{[\frac{1}{3}+\frac{2}{3}(\frac{R}{R_{max}})^n]^{\frac{3}{2n}}} \qquad (6)$$

where V_{max}=118 km s^{-1}, R_{max}=17.8 kpc, and n=1.46 (paper I). Kennicutt examined how star formation compared to the gas density and the expected critical density within a collection of galaxies. He found that star formation, as traced by Hα emission, was correlated with the gas surface density (as traced by H I emission) and that star formation was suppressed when the gas surface density fell below a critical value.

Based on data from paper I, and using our Hα images, we carried out a similar analysis on NGC 925. From the H I data we derive an average velocity dispersion, c, of 10 km s^{-1} for NGC 925. The value of α should be close to one, because galaxies should be close to being thin, isothermal disks, although Kennicutt (1989) finds an α of 0.67 fits his data better. In figure 6 we show the critical surface density (Σ_{crit}) for three values of α and surface density of H I multiplied by 1.47, Σ_{gas}, (following the example of Kennicutt 1989 to account for the molecular component of the gas). We also plot the Hα emission normalized to its peak. The Hα and H I surface densities shownare azimuthal averages. We find the Hα surface brightness to be relatively constant throughout the galaxy before cutting off abruptly at about 15 kpc, whereas the gas surface densitydecreases slowly with radius out to 18 kpc. This suggests that star formation in NGC 925 is not directly correlated with the gas surface density on a global scale.

While the abrupt decline of Hα surface brightness occurs at the edge of our field of view, we can use the value of $\Sigma_{gas}/\Sigma_{crit}$ at this point to yield α. Looking figure 6, we see that a value of α of near 0.3 works best for NGC 925 as opposed to α=1 and α=0.67. In reality, the Hα emission may continue beyond the edge of our field of view, implying a lower value of α still. Regardless of the extent of Hα emission beyond the region we imaged, the star formation criterion found by Kennicutt (1989), α=0.67, does not hold for NGC 925; instead, a value of α closer to 0.3 is more appropriate. This has been found to be the case for other galaxies as well. Values of α around 0.3 have been found for dIrr galaxiesby Hunter, Elmegreen, & Baker (1998), and for low surface brightness dwarf galaxies by van Zee *et al.* (1997). This is evidence that star formation in NGC 925 is governed more by local conditions than by global instabilities; a property more typical of later type galaxies than NGC 925. This is not surprising as star formation can occur in any type galaxy even when such a criterion is not met (see Ferguson *et al.* 1998 for a discussion). Ferguson *et al.* find H II regions outside the cited limits to the optical disk in a sample of spiral galaxies. Their outer H II regions, and ours, lie on coherent spiral arms even at large radii.

A better analysis of star formation criteria in NGC 925 could be done using CO data to trace the molecular component of the gas and using a larger field-of-view CCD to better trace the full extent of the Hα emission in NGC 925.

4.2. Star Formation in the spiral arms of NGC 925

Comparing the H I distribution of Paper I with the Hα and broadband images of NGC 925 allows us to examine the nature of star formation in the galaxy. The star formation in NGC 925, as traced by the Hα emission, is found in two main regions. The largest star forming regions are located at the end of the southern spiral arm and in the bar. In addition, star formation occurs at a lower level throughout the southern spiral arm (although it may be partially obscured by dust). The northern arm has sporadic star formation near the bar, but very little elsewhere, except, perhaps, near the end of the arm on the east side of the galaxy. The lack of coherent star formation along the north arms is not surprising given the weak definition of the stellar and gaseous arms.

Figure 7 shows the Hα in red on the H I in blue. In general, the star formation is occurring on top of H I peaks and the Hα emission traces the H I spiral arms very closely. The coincidence between the two distributions is highly correlated across the entire galaxy, but the exceptions are quite interesting. Specifically, there is a sizable H II region on the northwest spiral arm near the bar which is sitting in a local H I depression. This is the only major H II region which is not associated with a H I peak. This could be due to the star formation depleting the H I in this region, ionizing it, or the H I hole could be filled with molecular gas.

Looking at the broadband BVR image with the H I contours (figure 8), we see that the peak H I does trace the optical emission (as well as the Hα emission), as expected. This figure clearly shows that the southern spiral arm is much stronger and more coherent than the northern arm in H I and optical emission. The north side of the galaxy shows more flocculent spiral structure and less intense star formation as compared to the south. The southern arm also has a prominent gap in optical emission in the middle of the arm, while it still has a large amount of H I. This may be due to a large dust lane crossing the arm at this position. These are not caused by inclination, as the southern part of the galaxy is the far side of the galaxy. You can also see the bluest regions of the galaxy are those where large H II regions exist, specifically at the end of the southern arm, and to the northeast of the bar (which is the end of one of the northern arms).

As our data is of sufficient resolution and photometric quality to address the question of triggering of star formation in spiral arms of late-type galaxies, we took cuts through various regions of the spiral arms and bar in NGC 925 (figure 10) to look for offsets between the peaks of emission in B, R, Hα, and H I (see Beckman & Cepa 1990). Figure 9 shows the location of these cuts. These cuts were $4''$ wide and of varying length (as shown in figure 9). They are roughly centered on the arms or bar. The emission is an average over the width of the cut and is normalized to the peak intensity of that band in the cuts.

Triggering is defined as an increase in the star formation efficiency in the arm versus the interarm region; it is not simply an increase in total star formation. An offset in the peaks would suggest there is an age gradient across the cut (in a dust free world). Beckman & Cepa (1990), for instance, see such a color gradient in NGC 7479 between the B and I bands. Dust, however, can produce a similar gradient due simply to an extinction gradient within the spiral arm (Elmegreen 1995). In addition, we can not determine if triggering is actually occurring in the arm solely from an age (or color) gradient; it is entirely possible to see a gradient without any triggering (cf. Elmegreen 1995). What we can say is that the absence of an offset between the peaks in B and R implies the lack of an age gradient in the underlying stellar population.

Cuts along the southern arm (figure 10a-d) show the optical emission is well-aligned with the H I across the arm for most of the length of the arm. Peaks in B and R are well-aligned. In general, the Hα peaks correlate with the broadband peaks, but not always with the H I peaks. There are regions with no Hα peaks, but with strong broadband emission. In addition, there are two noticeable instances of Hα peaks in H I depressions. These occur at $\pm 40''$ in cut c and in cut d at $40''$. Star formation in the south arm is located in large H II regions which tend to lie on the peak of the H I distribution.

Cuts across the north arms (figure 10e-g) of NGC 925 show a decidedly different phenomenon than those of the south arm. Cut e shows optical emission peaking in an H I depression at $-50''$. There is also some Hα emission peaking with the H I at $20''$. Other cuts across the north arms, such as cut f, show a correlation between the optical and gas peaks, while cut g shows an offset between the optical emission and the H I peaks. In the north arms, the star formation appears less prolific than in the southern arm and occurs in smaller H II regions which are less coherently placed than in the south of NGC 925. This suggests that the nature of the spiral pattern, and hence the star formation, in the north and south arms of NGC 925 are different, if not fundamentally, then in our perception of it. This type of asymmetry, with one spiral arm being dominant in a galaxy, is quite typical in later-type spiral galaxies, such as SBm's (Odewahn 1991, de Vaucouleurs & Freeman 1972). NGC 925 illustrates that these properties are not limited to SBm's, but are evident in earlier type spiral galaxies, although less prominently.

4.3. Star Formation in the bar of NGC 925

In general, LTBS tend to have gas-rich bars with star formation occurring throughout the bar (Phillips 1995). Friedli & Benz (1995) suggest that star formation occurs along the major axis of dynamically young bars, and is concentrated in the center or in rings of older bars. NGC 925's bar is quite gas-rich and has star formation occurring all along its major axis. Thus, the Friedli & Benz (1995) model would imply that NGC 925 has a young bar. The extremely blue center of NGC 925, compared with its outer region (see section 3), could indicate a dynamically young bar as well, one which has just recently started prolific star formation. On the other hand, it is possible that weak bars, such as NGC 925's, are simply inefficient at funneling gas into the galactic nucleus. Furthermore, because corotation is far out in the disk (Elmegreen *et al.* 1998), the spiral arms have a large reservoir of gas to drive towards the center of NGC 925. As there is no inner Lindblad resonance in NGC 925 (Elmegreen *et al.* 1998) where the gas would pile up, the bar would be well-supplied with gas for long-term star formation, and it may not be young at all.

The star formation in the bar appears to be offset somewhat from the H I peaks. Examining the bar region in figure 7, we find that there is a great deal of star formation on the north side of the bar that is systematically displaced away from the H I peaks. This is better illustrated by cuts h-k in figure 10. Furthermore, the minor axis cuts (i-k) show that the B and R peaks are systematically offset to the north of the H I peak. While there is a Hα peak aligned with the H I peak in cut j, the main optical emission is offset. This could be explained by dust extinction, depletion of the H I by star formation or ionization, the gas being in molecular form, or the bar being a wave phenomenon.

For this offset to be an extinction feature, some process must pile up the dust preferentially along one side of the bar. Dust lanes have been found in the bars of other galaxies, and their coherence is usually attributed to shocks occurring in these bars (see Athanassoula 1992 for a nice discussion). The bar of NGC 925, however, does not have strong streaming motions (paper I) which would be indicative of shocks. The dust appears to be in filaments in the bar region, and not in well defined lanes. Furthermore, some of the cuts perpendicular to the major axis of the bar do show star formation correlated with the H I peaks, but all of the cuts indicate that the stellar emission is downstream of the H I peaks. Extinction should affect both Hα emission and R band emission to a similar extent. As this is not evident in the cuts, it is improbable that dust is causing the apparent offset.

The major axis cut (h) shows the Hα peaking throughout the bar, with the gaps in emission likely due to the prolific dust content of the bar. However, the broadband optical peaks are concentrated in a H I depression. This may be due to the recent star formation and young stars evacuating or ionizing the H I in this region of the bar. The H I depression in the bar could be filled with molecular gas, and not truly be depleted of all gas. Along the major axis of the bar the H I seems to be piled up at the bar ends, particularly near the dynamical center of the galaxy at $50''$. Spectra of the bar taken with the DensePak instrument on WIYN are in hand and should yield insight into the nature of the ionized gas in the bar. Higher spatial resolution H I data will also help to untangle the dynamics of gas in the bar.

If the offset of H I south of the Hα in the bar is not caused by dust, or by young stars ionizing or otherwise clearing out the H I in the bar, or by the gas being in molecular form, then the bar could be a wave phenomenon. This may be linked to the offset dynamical center of the galaxy as reported in Paper I. The dynamical center is located on the west end of the bar, so the geometry and dynamics make sense for this scenario, with the star formation occurring downstream of the gaseous peaks and the stars even further downstream, provided that star formation is occurring as the gas moves through the wave

5. Discussion & Conclusions

We have observed NGC 925 using the WIYN telescope in B, V, R, and Hα filters to better understand the stellar distribution and star formation properties of the galaxy. We have compared these observations with previously described H I observations (Paper I) to get a nearly complete picture of the properties of NGC 925.

The global properties of NGC 925 are typical for a late-type spiral galaxy. It has an obvious bar, and two large spiral arms. The southern spiral arm is apparently much stronger than the northern arm, which is quite flocculent. The relative dominance of the southern arm is apparent both optically and in the H I (paper I). This difference between the northern and southern spiral arms is not the only asymmetry present in the galaxy. The center of the galaxy, as derived from the outer isophotes, is coincident with the dynamical center (Paper I), but not with the center of the bar. These properties are typically associated with barred Magellanic spirals (de Vaucouleurs & Freeman 1972), although in the case of SBm's the offset bar and single, dominant spiral arm tend to be much more pronounced than they are in the case of NGC 925. Nevertheless, we see that such properties are not limited to Magellanic spirals, but are present in more subtle ways in earlier-type spirals. The optical properties of NGC 925, such as mass-to-light ratio and absolute magnitude, are as would be expected for a typical late-type galaxy.

From our isophote fitting, we find that NGC 925's surface brightness distribution can be characterized by a double exponential; one for the bar and one for the outer disk. The bar is quite easily distinguished from the rest of the galaxy in the fits, by having a well-defined center, position angle, and ellipticity differing from the outer disk.

The bar also has a exponential brightness distribution with a scale-length much smaller than the rest of the galaxy. There is little evidence that the bar has any effect on the structure of the rest of the galaxy. The isophote fits show quite a bit of structure outside of the bar region. This is almost certainly due to the bright southern spiral arm, which shows up clearly as a surface brightness enhancement in the fits. At the same radius as this enhancement, we can see distinct changes in the fits for the center, ellipticity, and position angle. The fits do not seem to be affected by the weaker northern arm. This is further evidence for NGC 925's similarity to the SBm one-armed spiral pattern. The fits also show that NGC 925 gets redder with increasing radius, atypical of normal spiral galaxies in the field. This could indicate a recent enhancement of star formation in the inner galaxy.

From our analysis of the critical density for massive star formation in NGC 925, using the technique of Kennicutt (1989), we find that the galaxy has widespread star formation occurring outside of the radius where it should be suppressed. NGC 925 has a very flat Hα surface brightness distribution, with emission extending all the way to the edge of our image at 15 kpc. Kennicutt (1989) using a sample of 15 Sc galaxies found that star formation was suppressed when α=$\Sigma_{gas}/\Sigma_{crit}$ fell below 0.67. For NGC 925 star formation continues past this radius and is more consistent with an α $\sim$0.3, like what was found by Hunter *et al.* (1998) and van Zee *et al.* (1997) for later-type galaxies. The exact value of α is unclear, but probably lower, as the Hα emission could continue beyond our field of view.

As mentioned above, the spiral arms in NGC 925 are quite different. The north arm is quite weak, lacks coherence, and has only patchy star formation. The southern arm, on the other hand, can be traced all the way from the bar out to the edge of the galaxy and has plenty of star formation. Aside from a small gap, the arm is quite coherent. There is a long dust lane associated with the southern arm, which probably obscures some star formation. If there is dust along the northern arm, it is not nearly so well-behaved. Taking cuts across the northern and southern arms, we can measure the relative positions of the stars, H II regions, and H I. In the southern arm, the strongest Hα and stellar emission is closely aligned with the peak of the H I. Large scale coherence breaks down in the northern half of the disk. At some places (40-50$''$ in cut f) star formation is well correlated with peaks in the H I distribution. At other locations ($\sim$40$''$ in cut g) star formation is displaced off of the H I peaks while elsewhere the H I and Hα are anti-correlated (e.g. $\sim$50$''$ in cut e). The difference between the north and south arms suggests that there may be some fundamental difference in the nature of the two arms.

Using the same cuts, we looked for evidence of triggering by the spiral arms. If there is triggering in the arms, we might expect a color gradient (implying an underlying age gradient) perpendicular to the arms. Such a color gradient can also be caused by dust extinction. The lack of a color gradient would imply the lack of an age gradient, and, hence a lack of triggering. While the cuts of the north arms show that the stellar emission is typically offset from the Hα and H I emission, there is no offset present between the B & R peaks. Similarly, the southern arm shows no offset between the broadband emission peaks. The lack of an offset shows that there is no color gradient, and hence it is unlikely that an age gradient due to triggering in the spiral arm is occurring. This suggests that there is no larger scale organization of the star formation in the northern disk–a result reminiscent of irregular galaxies. Star formation must be driven by local conditions and processes in the northern half, while larger scale phenomena organize star formation in the bar and southern arm.

Finally, we examined the nature of the NGC 925's bar and the star formation occurring within it. As is expected for late-type bars (Phillips 1995), NGC 925 has star formation occurring all along the bar. Cuts perpendicular to the major axis of the bar show that the star formation is occurring along the major axis, but the broadband optical emission is systematically offset to the north of the H I peaks. While this could be a dust effect, we would expect the Hα emission to be similarly affected, but it is not. This could also be due to the massive star formation in the bar ionizing or clearing out the H I in the bar. The systematic offset may be related to the dynamical center being offset from the bar center, and hence the bar could be a wave pattern moving through the gaseous medium in NGC 925. We might expect to see the peak of the stellar emission downstream of the star formation, as is the case here. It may be that the bar of NGC 925 is not actually a bar, but has more in common with the spiral arms of NGC 925.

Overall, this study has shown that NGC 925 is a prototypical late-type spiral galaxy, with some properties that are characteristic of Magellanic spirals, such as an off-center bar and a dominant spiral arm. These traits are less pronounced in NGC 925 than in an SBm indicating a probable smooth transition of these properties from Scd galaxies to Sm's. Massive star formation in NGC 925 persists beyond the radius predicted by Kennicutt (1989) for late-type spirals, but behaves more like dIrr's (Hunter *et al.* 1998). This result may be exacerbated by wider field imaging of NGC 925, however, and star formation almost certainly continues at a low level beyond this point (see Ferguson *et al.* 1998 for an example). The north and south arms are not only different in brightness, but in coherence and in the distribution of stars across the arms. The north arm has stars offset from H I peaks, while the south arm has both star formation and stellar emission coincident with the neutral gas peaks. Finally, the bar of NGC 925 appears to be a typical late-type bar being gas-rich and having star formation throughout, but the stars are offset from the Hα and H I peaks. This fact coupled with the offset dynamical center of NGC 925 suggests that the bar may be more of a wave phenomenon, similar to a spiral arm.

The authors would like to thank the staff at the WIYN observatory and on Kitt Peak for helping make our observing run go smoothly, and for their excellent assistance in producing the wonderful data from the WIYN telescope. The authors also thank the anonymous referee for comments improving the quality of this paper. This work was partially supported by NSF grant AST 96-16907 to E.M.W. This research has made use of the NASA/IPAC Extragalactic Database (NED) which is operated by the Jet Propulsion Laboratory, California Institute of Technology, under contract with the National Aeronautics and Space Administration.

REFERENCES

Athanassoula, E. 1992, MNRAS, 259, 345.

Beckman, J.E., & Cepa, J., 1990, A&A, 229, 37.

de Vaucouleurs, G., & Freeman, K. 1972, Vistas Astron., 14, 163.

de Vaucouleurs, G., de Vaucouleurs, A., Corwin Jr., H.G., Buta, R.J., Paturel, G., Fouque, P. 1991, Third Reference Catalog of Bright Galaxies (RC3) (New York: Springer).

Elmegreen, B.G., 1995, “The Formation of the Milky Way.”, eds. E.J. Alfaro, & A.J. Delgado, 42.

Elmegreen, B.G., & Elmegreen, D.M. 1985, ApJ, 370, 438.

Elmegreen, B.G., & Elmegreen, D.M. 1989, ApJ, 342, 677.

Elmegreen, B.G., & Elmegreen, D.M., 1990, ApJ, 355, 52.

Elmegreen, B.G., Elmegreen, D.M., & Montenegro, L., 1992, ApJS, 79, 37.

Elmegreen, B.G., Wilcots, E.M., & Pisano, D.J., 1998, ApJ, 494, 37L.

Ferguson, A.M.N., Gallagher, J.S., & Wyse, R.F.G., 1998, AJ, 116, 673.

Friedli, D., & Benz, W., 1995, A&A, 301, 649.

Hunter, D.A., Elmegreen, B.G., & Baker, A.L., 1998, ApJ, 493, 595.

James, R.A., & Sellwood, J.A. 1978, MNRAS, 182, 331.

Kennicutt, R.C., 1989, ApJ, 344, 685.

Landolt, A.U. , 1992, AJ, 104, 340.

Levine, S.E., & Sparke, L.S., 1998, ApJ, 496, L13.

Martin, P., & Roy, J-R. 1994, ApJ, 424, 599.

Massey, P., Strobel, K., Barnes, J.V., & Anderson, E., 1988, ApJ, 328 ,315.

Matsuda, T., & Nelson, A.H., 1977, Nature, 266, 607.

Odewahn, S., 1991, AJ, 101, 829.

Phillips, A.C., 1995, “Barred Galaxies”, eds. R. Buta, D.A., Crocker, & B.G. Elmegreen, 44.

Pisano, D.J., Wilcots, E.M., & Elmegreen, B.G., 1998, AJ, 115, 975. (Paper I).

Roberts, M.S, & Haynes, M.P., 1994, ARA&A, 32, 115.

Sanders, R.H., & Huntley, J.M. 1976, ApJ, 209, 53.

Silbermann, N.A., *et al.* 1996, ApJ, 470, 1.

Sellwood, J.A., & Sparke, L.S. 1988, MNRAS, 231, 25.

van Zee, L., Haynes, M.P., Salzer, J.J., & Broeils, A.H., 1997, AJ, 113, 1618.

Vennik, J., Hopp, U., Kovachev, B., Kuhn, B., & Elsässer, H., 1996, A&AS, 117, 261.

Figure Captions

Fig. 1.—

A combined B,V,R image from the WIYN 3.5m telescope. B is represented by blue, V by green, and R by red.

Fig. 2.—

The results from the isophote fitting of NGC 925. Counter-clockwise from upper left they are Right Ascension of center, Declination of center, ellipticity, and position angle. Blue represents fits to the B band image, Green for V, and Red for R.

Fig. 3.—

The results of the isophote fits to the surface brightness in B,V,R for NGC 925. The colors are the same as figure 2. The upper panel shows the data on an arbitrary scale (points) and the fits to the bar and disk (solid lines). The middle panel shows the residuals from just the disk fit. The lower panel shows the residuals from both the bar & disk fits. The solid line in the lower 2 panels mark the zero level.

Fig. 4.—

A representation of the model isophotes as fit to the R band image of NGC 925. Ellipses are plotted for one out of every three annuli. They illustrate the relative location and orientation of each annulus, but do not reflect the surface brightness distribution.

Fig. 5.—

This plot shows 4 centers of NGC 925: the center of NGC 925 according to the RC3 (RC3), the center of the bar (B), the center of the outer isophotes (ISO), and the dynamical center (DYN). The boxes represent the derived errors to the fitted centers. The ellipse is the FWHM of the beam from the H I observations in paper I.

Fig. 6.—

a) Top panel is a plot of gas surface density (solid line), as measured by H I observations from paper I, and multiplied by 1.47 to account for molecular gas. The dashed line is the critical gas surface density for collapse an α=1. The dot-dash line is the radial Hα distribution normalized to its peak. The vertical dotted line indicates the nearest edge of the chip from the center of the bar of

---

This 2-column preprint was prepared with the AAS LaTeX macros v5.0.

NGC 925. The bottom panel indicates the ratio of the measured gas surface density to the critical density. The horizontal dotted line is the level when massive star formation should cease. The vertical horizontal line is the same as in the top panel. b) same as in a, but for α=0.67. c) same as a, but for α=0.3.

Fig. 7.—

This figure shows the Hα emission from NGC 925 (in red) and the H I emission (in blue) overlaid on each other. Regions that are white are where there are peaks in both Hα and H I.

Fig. 8.—

This figure shows the H I contours from paper I (in yellow) overlaid on the combined B,V,R WIYN image from figure 1. Hatched contours indicate a H I depression. The H I beam is shown in the lower right.

Fig. 9.—

This is an optical R band image of NGC 925, with the location of the cuts marked on it. The rectangular boxes are show the region over which the cut was taken. The letters correspond to the cuts shown in figure 10, and also marks the most positive point in the cut.

Fig. 10.—

The results of the cuts across the southern arm, northern arms, and bar of NGC 925. Each band of observations is normalized to its peak. The solid line is B band, the dashed line is R, the dot-dash line is Hα, and the dotted line is H I column density. Cuts a-d are for the southern arm. Cuts e-g are for the northern arms. Cut h is the bar major axis, and cuts i-k are parallel to the bar minor axis. The most positive points in the cuts are marked by the letters in figure 9.

This figure "figure1.jpg" is available in "jpg" format from:

http://arXiv.org/ps/astro-ph/0004219v1

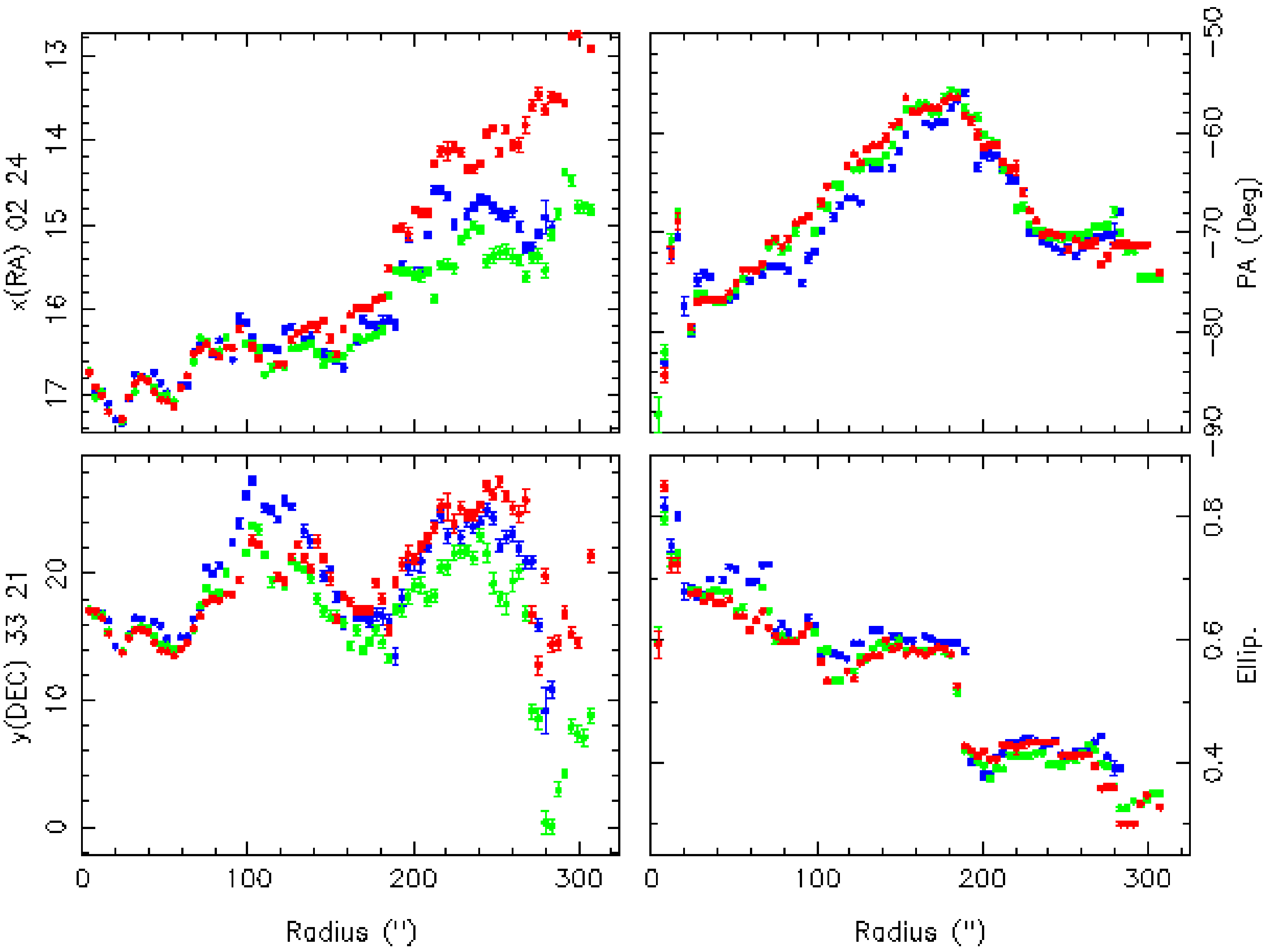
x(RA) 02 24
13
14
15
16
17
PA (Deg)
−50
−60
−70
−80
−90
y(DEC) 33 21
0
10
20
Ellip.
0.4
0.6
0.8
0
100
200
300
Radius ('')
Radius ('')

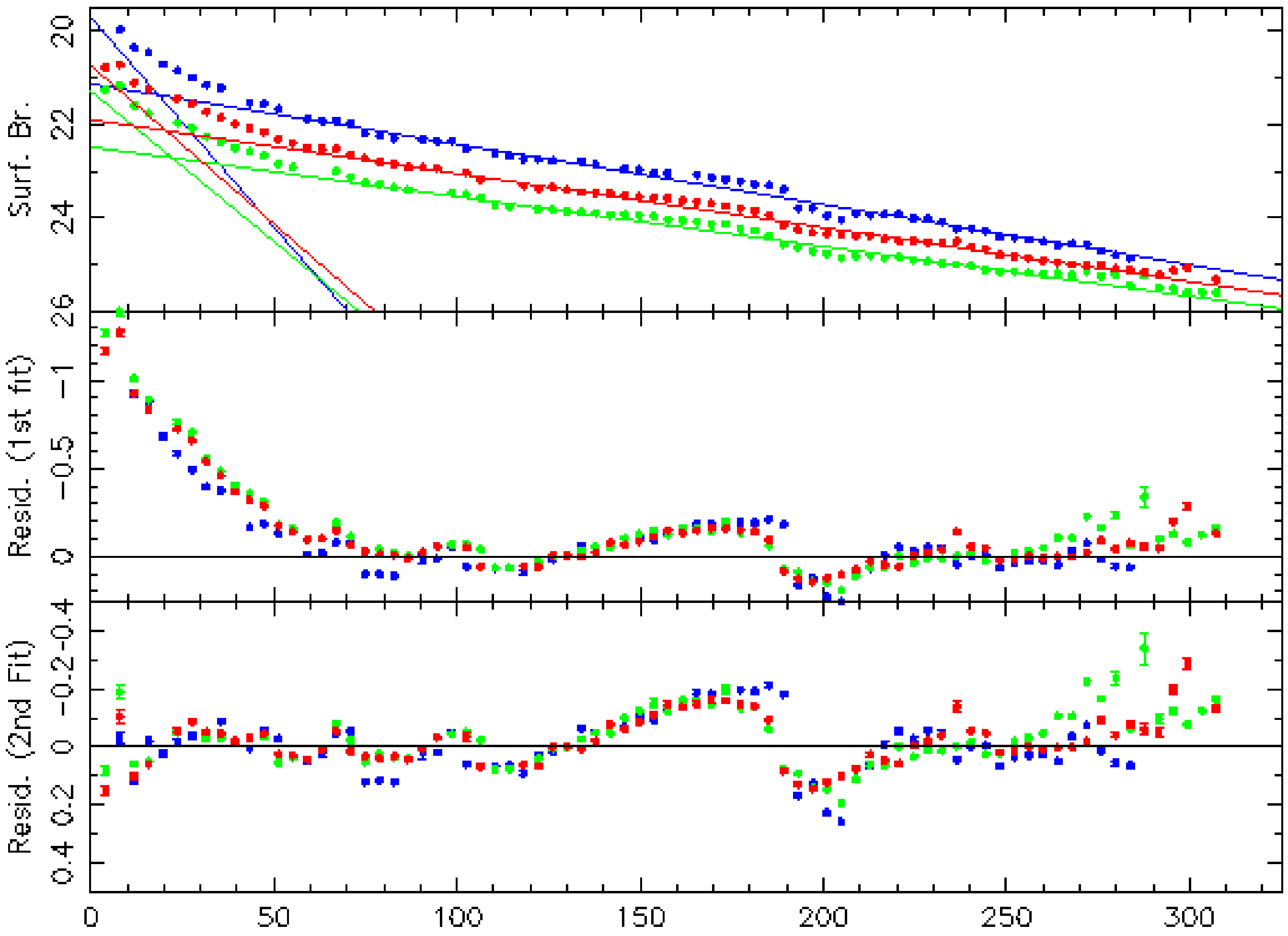
Surf. Br.
20
22
24
26
Resid. (1st fit)
−1
−0.5
0
Resid. (2nd Fit)
−0.4
−0.2
0
0.2
0.4
0
50
100
150
200
250
300

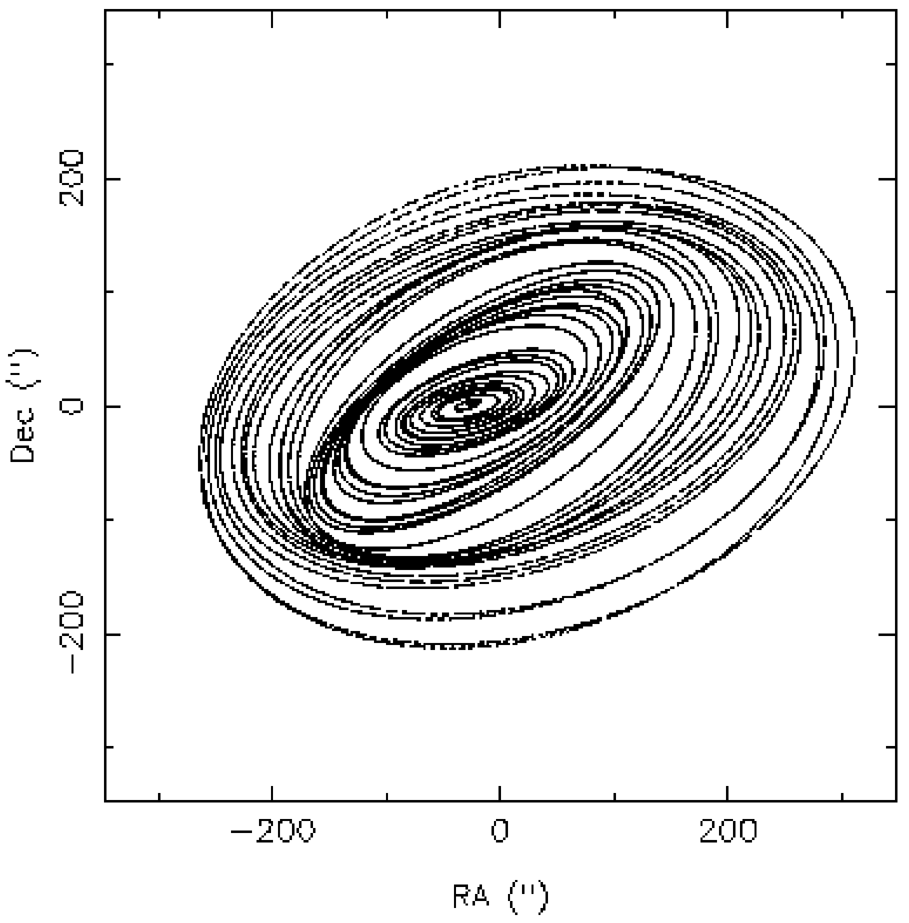
Dec (")
200
0
−200
−200
0
200
RA (")

This figure "figure5.jpg" is available in "jpg" format from:

http://arXiv.org/ps/astro-ph/0004219v1

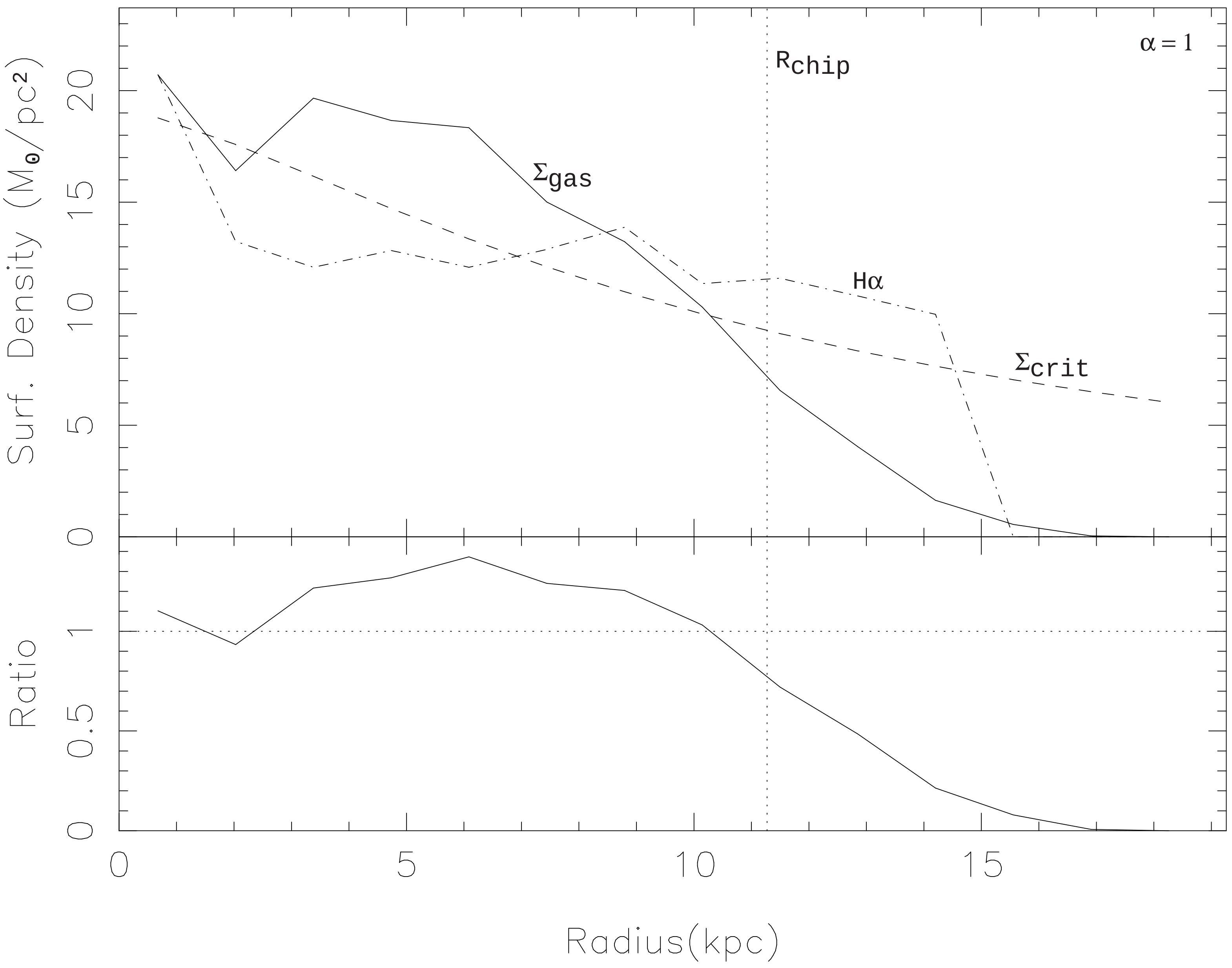
α = 1
R_chip
Σgas
Hα
Σcrit
Surf. Density (M⊙/pc²)
0
5
10
15
20
Ratio
0
0.5
1
0
5
10
15
Radius(kpc)

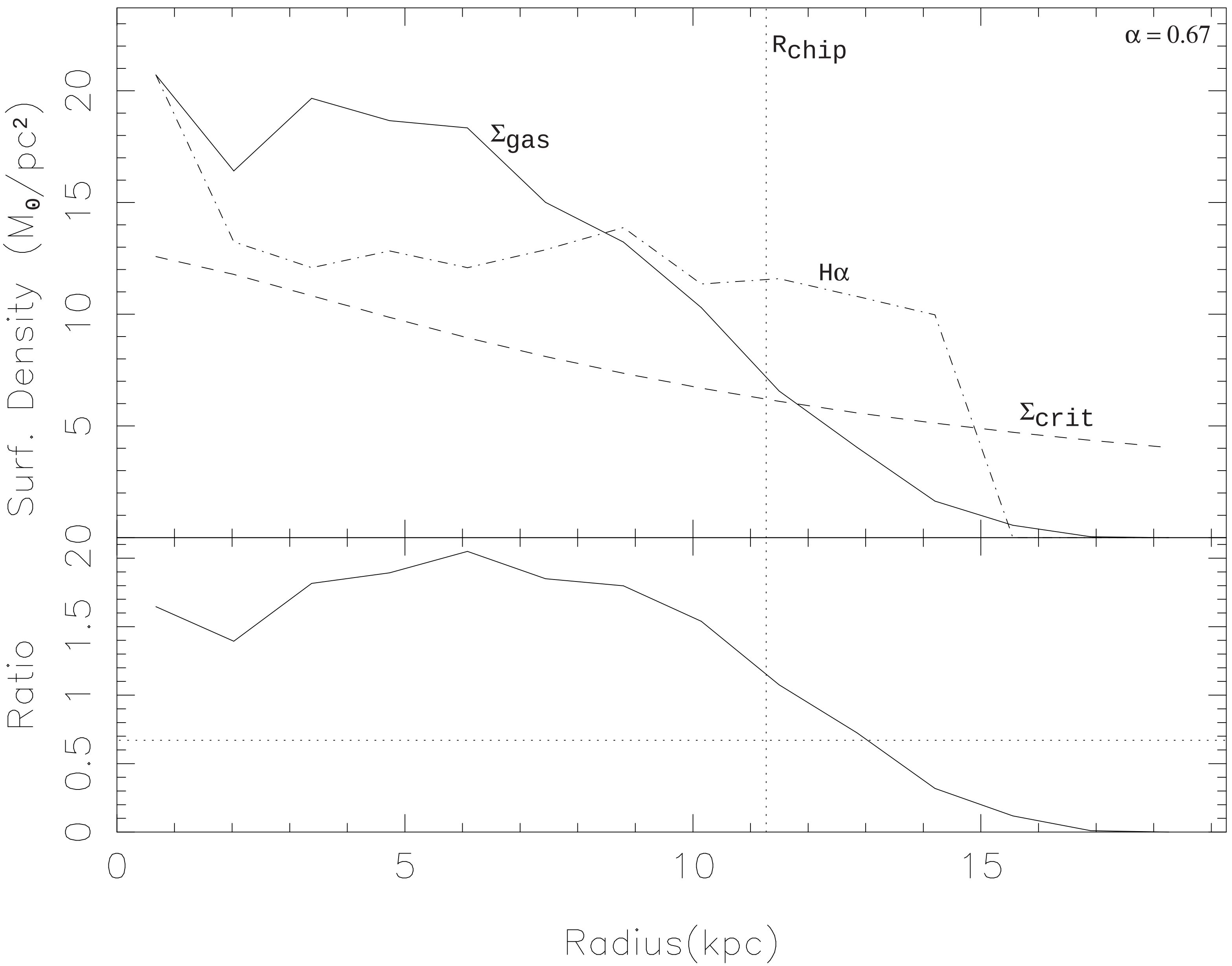

α = 0.67
R_{chip}
Σ_{gas}
Hα
Σ_{crit}
Surf. Density ($M_{\odot}/pc^2$)
0
5
10
15
20
Ratio
0
0.5
1
1.5
2
0
5
10
15
Radius(kpc)

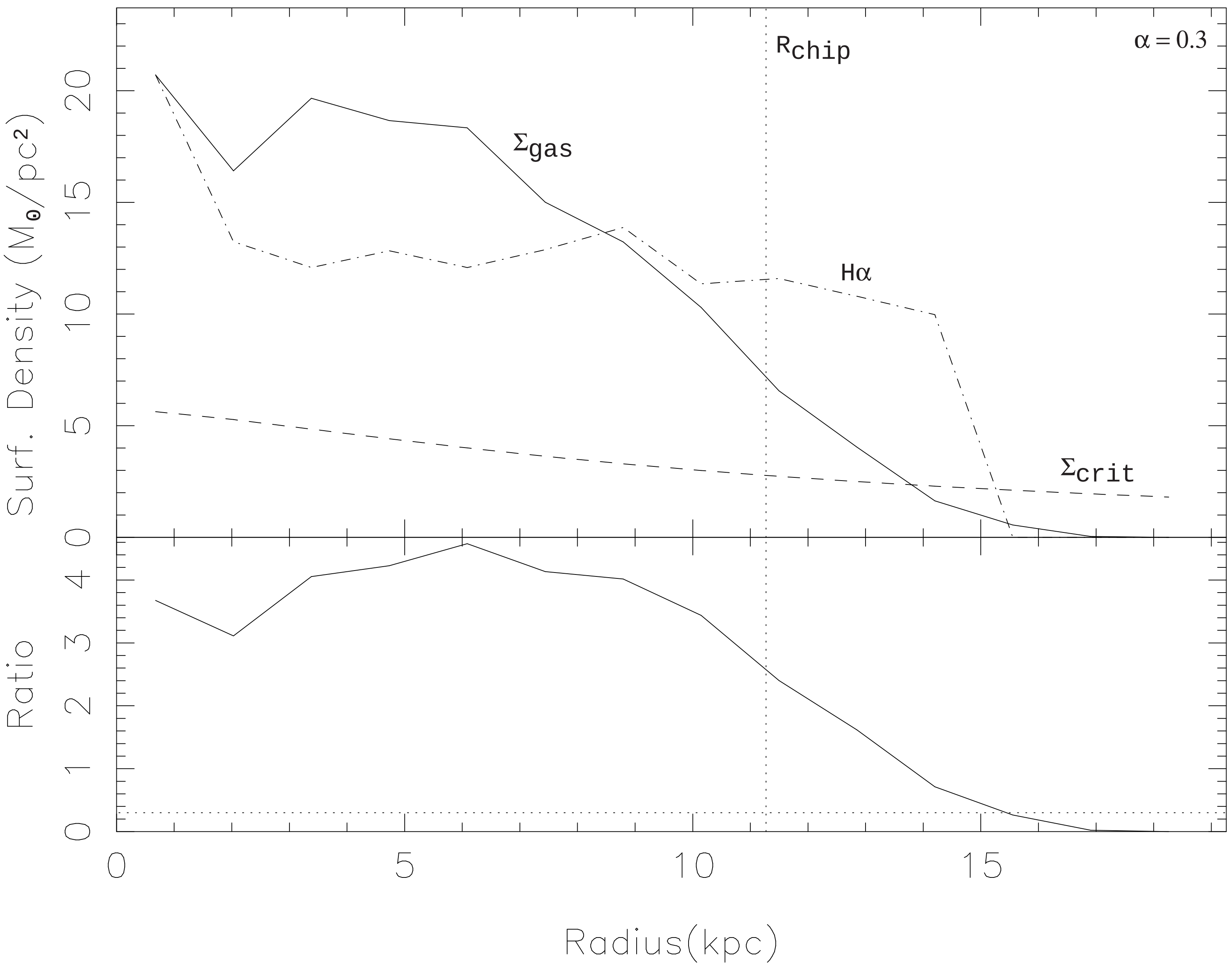
α = 0.3
R_chip
Σ_gas
Hα
Σ_crit
Surf. Density (M_⊙/pc²)
0
5
10
15
20
Ratio
0
1
2
3
4
0
5
10
15
Radius(kpc)

This figure "figure7.jpg" is available in "jpg" format from:

http://arXiv.org/ps/astro-ph/0004219v1

This figure "figure8.jpg" is available in "jpg" format from:

http://arXiv.org/ps/astro-ph/0004219v1

This figure "figure9.jpg" is available in "jpg" format from:

http://arXiv.org/ps/astro-ph/0004219v1

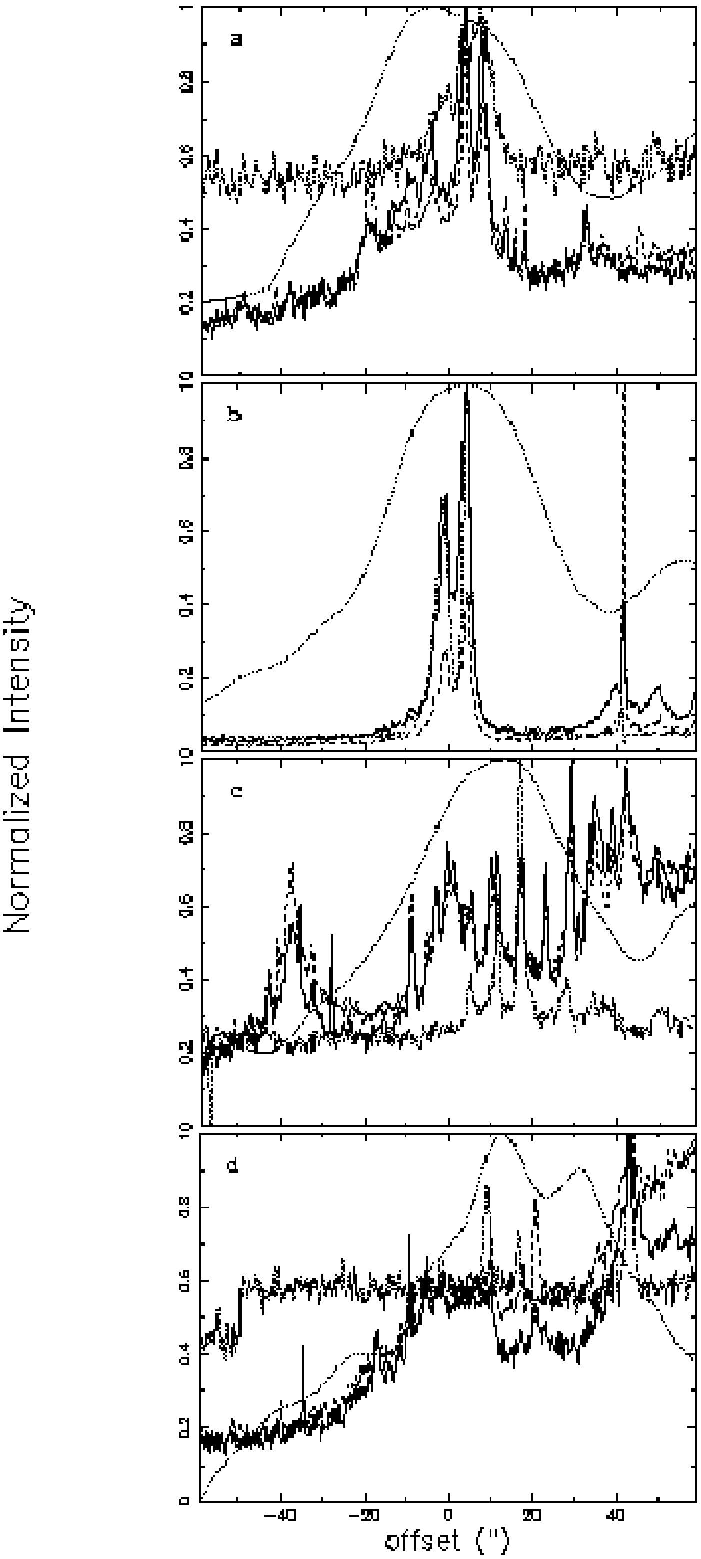
a
b
c
d
Normalized Intensity
offset (")
-40
-20
0
20
40
0
0.2
0.4
0.6
0.8
1.0

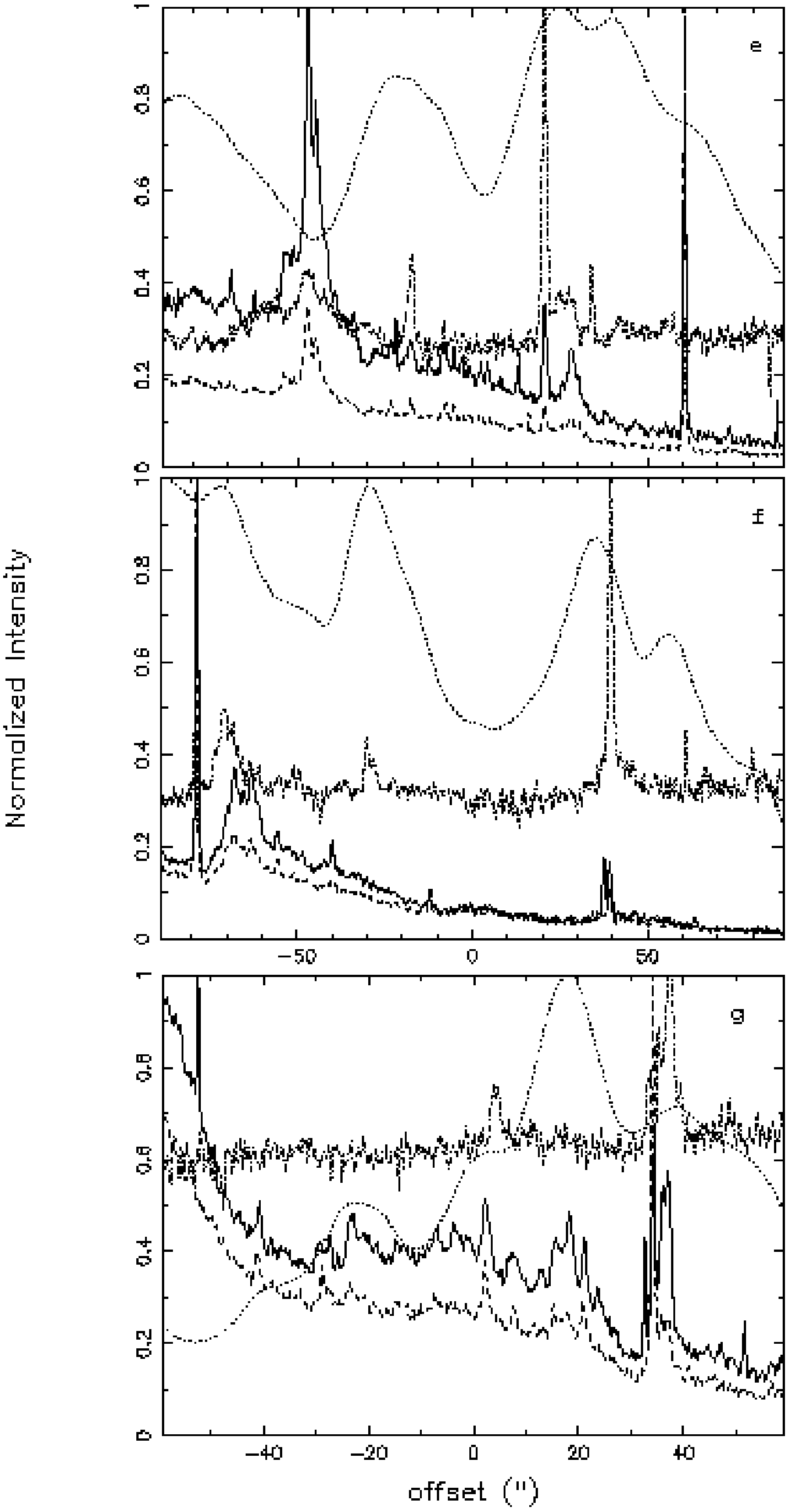
e
f
g
Normalized Intensity
0
0.2
0.4
0.6
0.8
1
-50
0
50
-40
-20
0
20
40
offset (")

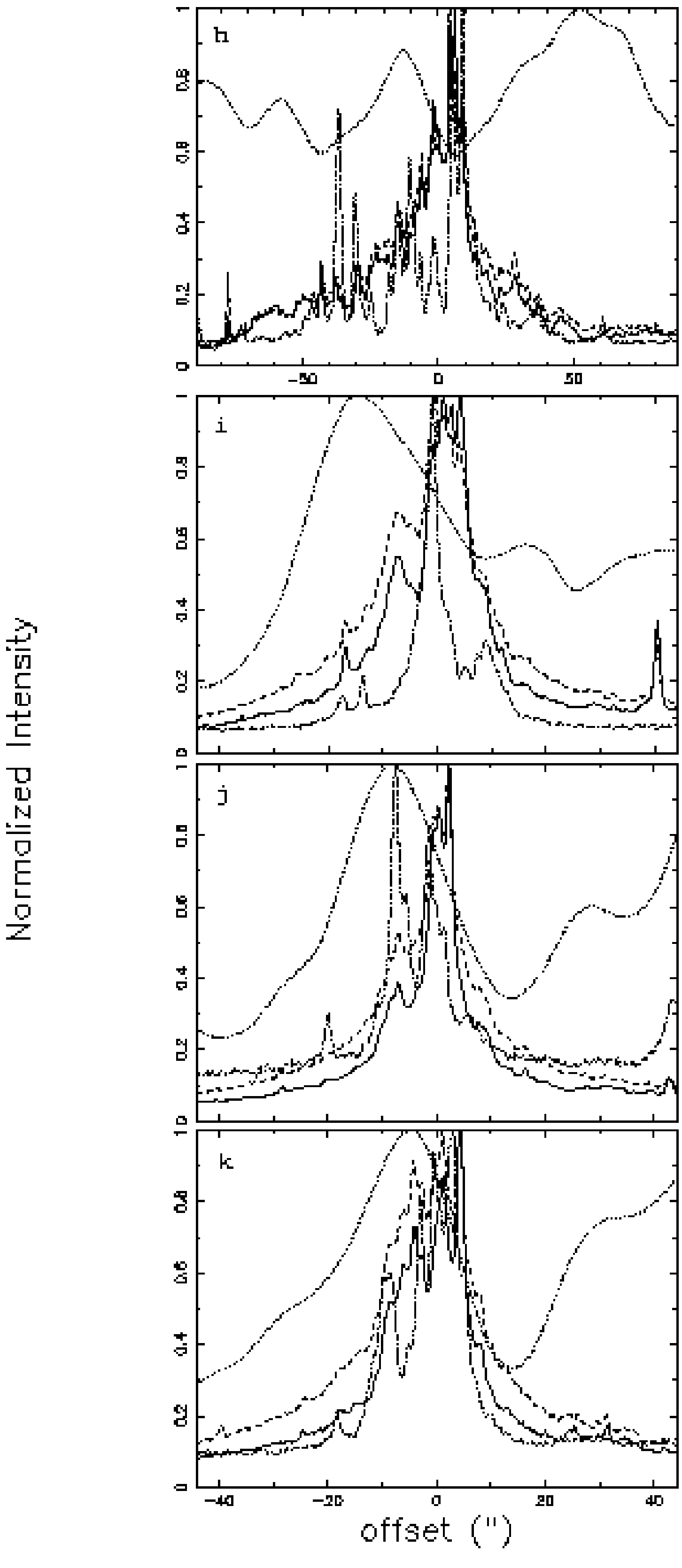
h
i
j
k
Normalized Intensity
offset (")
0
0.2
0.4
0.6
0.8
1
-50
0
50
-40
-20
0
20
40

Table 1. NGC 925 Properties

Property	Value
Hubble Type[a]	SAB(s)d
Distance[b](Mpc)	9.3
D_{25}[c](kpc)	28
M_B[a](mag)	-19.9
L_B ($L_\odot$)	1.4×10^{10}
M_{HI}[e]($M_\odot$)	5×10^9
M_{tot}[e]($M_\odot$)	7×10^{10}
M_{HI}/L_B ($M_\odot/L_\odot$)	0.36
M_{tot}/L_B ($M_\odot/L_\odot$)	5.0

[a] from NED

[b] from Silbermann *et al.* 1996

[c] from RC3

[d] paper I

Table 2. Observing Properties

Filter	Exp. Time[a]	Seeing[a]	Date
Harris B	600s, 600s	0.6″, 0.7″	Oct. 7, 1996
Harris V	600s, 600s	0.55″, 0.7″	Oct. 7, 1996
Harris R	600s, 600s	0.5″, 0.7″	Oct. 7, 1996
Hα (6565/47)	2×1200s, 2×1200s	1″, 1″	Oct. 6, 1996
Hα-off (6653/68)	900s, 900s	1″, 1″	Oct. 6, 1996

[a] The two values are for the West and East sides of NGC 925 respectively.

Table 3. Isophote Fitting Results[a]

Parameter	Bar[b]	Outer Disk[c]
Center:		
α (1950)	2:24:17.0±0.2	2:24:14.8±0.6
δ (1950)	33:21:15±1	33:21:23±2.5
Position Angle (^{o})	-75±3	-68±4
Ellipticity	0.69±0.03	0.42±0.02
Inclination[d](^{o})	72±2	55±2
Scale-length (kpc)		
B	0.544	3.78
V	0.758	4.58
R	0.720	4.23
μ_o[e](mag)		
B	19.7	21.1
V	21.3	22.5
R	20.7	21.9

[a] an average of all bands, except where noted

[b] From fit within 60″.

[c] From fit between 200″ & 270″

[d] Derived from ellipticity.

[e] In the same arbitrary units as in figure 3.